Probing the kinesin reaction cycle with a 2D optical force clamp

Steven M. Block*†‡, Charles L. Asbury*, Joshua W. Shaevitz§, and Matthew J. Lang*¶

Departments of *Biological Sciences, †Applied Physics, and §Physics, Stanford University, Stanford, CA 94305

With every step it takes, the kinesin motor undergoes a mechano-chemical reaction cycle that includes the hydrolysis of one ATP molecule, ADP/P_i release, plus an unknown number of additional transitions. Kinesin velocity depends on both the magnitude and the direction of the applied load. Using specialized apparatus, we subjected single kinesin molecules to forces in differing directions. Sideways and forward loads up to 8 pN exert only a weak effect, whereas comparable forces applied in the backward direction lead to stall. This strong directional bias suggests that the primary working stroke is closely aligned with the microtubule axis. Sideways loads slow the motor asymmetrically, but only at higher ATP levels, revealing the presence of additional, load-dependent transitions late in the cycle. Fluctuation analysis shows that the cycle contains at least four transitions, and confirms that hydrolysis remains tightly coupled to stepping. Together, our findings pose challenges for models of kinesin motion.

In the study of kinesin motility, the working hypothesis has been that only a small number of transitions in the mechanochemical reaction cycle (perhaps just one) are associated with motion and force production. In support of this hypothesis, reaction pathways that incorporate a single load-dependent transition can account globally for force-velocity and [ATP]-velocity curves measured under backward loading (1). Working strokes that might correspond to such a transition have been reported for the kinesin-like motor Ncd (2), and proposed for single-headed kinesin constructs [i.e., the neck-linker "zippering" hypothesized by Rice *et al.* (3)]. But the apparent stroke distance falls short of the 8-nm-sized steps that processive kinesin dimers make when they move along the microtubule lattice (4), raising the question of whether a second conformational change might occur elsewhere in the reaction cycle that makes up the difference. If so, where? Moreover, the free energy available for zippering of the neck-linker is on the order of $k_B T$ (5), and seems to be too low to account for kinesin's ability to generate steps under load [which requires up to ≈50 pN·nm (6)]. Given the uncertainties, the nature of the putative working stroke remains controversial.

To test the "one-stroke" hypothesis, we studied the dependence of kinesin motility on the magnitude and direction of load at various ATP concentrations, by using a recently developed 2D optical force clamp (7). This instrument can record long records of the motion of individual kinesin molecules under fixed forces applied in any azimuthal direction (see Fig. 1), and is therefore ideally suited to study motor kinetics under load. Experimentally, kinesin velocity obeys Michaelis–Menten (MM) kinetics (8–11), where the parameters for the turnover rate, k_{cat}, and the apparent binding constant for substrate, k_b, reflect the combined effects of the underlying microscopic rate constants, k_i, that comprise the full enzymatic cycle. Certain transition rates in any cycle will contribute solely to k_b whereas others will contribute to both k_{cat} and k_b (we call these "overlap rates"), and, depending on particulars of the reaction scheme, there can also be rates that solely contribute to k_{cat}. If motion and force production occur during a single transition in the kinesin cycle, then applied load will affect the kinetics in predictable ways. Measuring how k_{cat} and k_b vary with force therefore provides a means to test the one-stroke model and can supply information about where other

force-dependent transitions may reside in the overall reaction pathway (Fig. 2).

A one-stroke mechanism is consistent with the experimental data for the relatively strong effects of longitudinal load. However, weaker force dependencies must occur elsewhere in the cycle to account for the observed effects of sideways loads.

Materials and Methods

Assays. Motility assays were performed essentially as described (8). Briefly, 0.5-μm-diameter silica beads were mixed with native kinesin [purified from *Loligo pealei* (12)] at sufficiently low concentration such that fewer than one kinesin molecule, on average, was bound to each bead. Kinesin bead incubations were performed for >30 min in a buffer containing 80 mM Pipes (pH 6.9), 50 mM potassium acetate, 4 mM $MgCl_2$, 2 mM DTT, 1 mM EGTA, 7 μM Taxol, and various ATP concentrations. Up to 100 μg·ml^{-1} casein was added after incubation, as a blocking protein. An oxygen-scavenging system (250 μg·ml^{-1} glucose oxidase, 30 μg·ml^{-1} catalase, 4.5 mg·ml^{-1} glucose) was added to the kinesin-beads just before measurement. Beads were optically trapped and held near microtubules (polymerized from purified bovine brain tubulin; Cytoskeleton, Denver) that had been immobilized on a polylysine-coated glass coverslip. Measurements of displacement were made by using an optical force clamp apparatus that can apply constant, piconewton forces in any chosen azimuthal direction to the moving beads (below). To ensure work in the single molecule regime, data only from assays in which fewer than half the tested beads moved were analyzed. All chemicals were from Sigma, except glucose oxidase and catalase (Calbiochem) and DTT (GIBCO/BRL).

Instrumentation and Calibration. Constant forces in two dimensions were applied to the moving beads by using a recently developed 2D optical force clamp (described in detail in ref. 7). Briefly, the instrument is based on an inverted microscope (Eclipse TE200; Nikon) modified for mechanical stability and the incorporation of three lasers for (*i*) trapping (1,064 nm; Spectra-Physics), (*ii*) position detection (828 nm; Point Source, Southampton, U.K.), and (*iii*) total internal reflection fluorescence excitation (not used here). Position detection was accomplished by focusing the low-power detection laser onto the trapped bead and monitoring the deflected light in a plane conjugate to the back focal plane of the microscope condenser by using a quadrant photodiode. Software written in LABVIEW 6I (National Instruments, Austin, TX) was used to control the trap position (via acousto-optical deflectors; IntraAction, Bellwood, IL) and specimen position (using a precision 3-axis stage; Physik Instrumente, Karlsruhe/Palmbach, Germany), permitting many aspects of the experiments to be automated. The 2D position
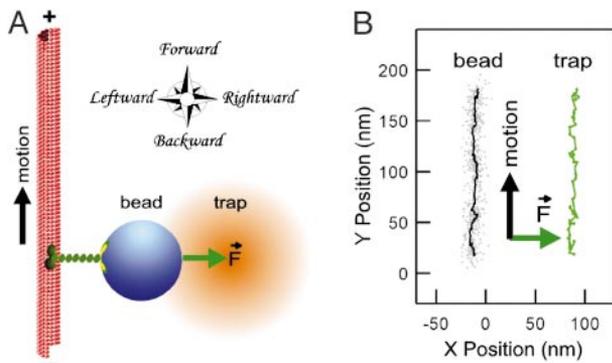
BIOPHYSICS

Fig. 1. Operation of the 2D optical force clamp. (*A*) A cartoon illustrating the application of forces in two dimensions to single kinesin motors in our experimental geometry (not to scale). During an experiment, both the microscope stage (microtubule, red) and optical trap (orange) are moved dynamically to maintain constant force on the bead (blue), and thereby on the kinesin molecule (green) (7). A Cartesian sign convention based on the normal (plus-end directed) movement of native kinesin on the microtubule was adopted: forces applied forwards or to the right are considered positive, whereas forces applied rearwards or to the left are considered negative. (*B*) Sample *x-y* plot of experimental data for a run obtained under a constant rightward load of 4.8 pN. During the run, the bead and trap moved together, but laterally offset, from the bottom of the frame toward the top.

Fig. 2. Model of the kinesin mechanochemical cycle. (*A Left*) A schematic diagram illustrating how force affects the transition rates involving motion. The application of load tilts the energy landscape (shown as a contour plot) along the direction of loading, changing the passage rate over the barrier according to the relation shown, where $\vec{F} \cdot \vec{\delta}_i$ is the dot product of the force vector, $\vec{F}$, and the vector from the starting to the transition state, $\vec{\delta}_i$, pointing along the reaction coordinate. (*A Right*) Rate constants derived from a global fit of this reaction scheme to the data of Figs. 3 and 4 (see *Materials and Methods*). (*B*) A hypothetical five-state reaction scheme in which the transitions from 1→4 (blue rectangle) contribute to the MM parameter k_b, whereas the transitions from 2→1 (red rectangle) contribute to k_{cat}. The transition from 2↔3 involves a relatively large motion along the microtubule, whereas transitions from 4→5 and 5→1 involve smaller motions perpendicular to the microtubule that are equal in magnitude and opposite in direction.

detector response was mapped, and trap stiffnesses were measured along the two principle axes each time a new bead was selected. Each bead was then placed over a microtubule and at the edge of the calibrated zone of the detection system by using automated, precision routines for vertical and lateral positioning (7). The force clamp feedback was triggered once the bead was pulled into the calibrated zone of the detector. During clamping, bead position was sampled at 20 kHz (after anti-alias filtering to 10 kHz) while the trap position was updated at 200 Hz to maintain the desired load. For sideways and forward loads, a compensatory movement of the specimen stage at the onset of trapping kept the bead within the detection zone. Bead position data were decimated to 2 kHz before storing to disk. To minimize force errors associated with Brownian movements of the bead or small drifts in the position detection system, trap stiffness was always chosen so that a bead-trap separation of 100 nm was achieved at the desired load, except for the very lowest longitudinal force of ±0.51 pN, for which this separation was 50 nm.

Data Analysis. At least 58 individual records of kinesin motion were obtained at every force condition and ATP concentration studied (≥29 for each of two possible microtubule orientations; see below). Mean velocities and randomness values were computed from the records as follows, by using software written in IGOR PRO 4.0 (WaveMetrics, Lake Oswego, OR). For each run obtained under forward or backward loading, the slopes of line-fits to the *x*- and *y*-displacement data vs. time were added in quadrature to compute the run velocity. The mean velocity, ⟨*v*⟩, and SEM were obtained from a weighted Gaussian fit to the histogram of these individual run velocities (which were normally distributed). To calculate the randomness, pairwise distances between all measured *y*-positions in a given record were used to generate a running plot of variance, $[y(t + \Delta t) - (y(t) + \langle v \rangle \Delta t)]^2$, vs. Δt. The variance increased linearly for time separations beyond 3.5 ms (a lower bound chosen to be safely longer than the correlation time of a bead held in the force clamp) and below 20 nm·⟨*v*⟩$^{-1}$. The slope of the line between these limits was then divided by *d*·⟨*v*⟩, where *d* is the 8.2-nm step size, to obtain the *r* parameter for the record. The global mean randomness and associated SE were obtained arithmetically from the individual
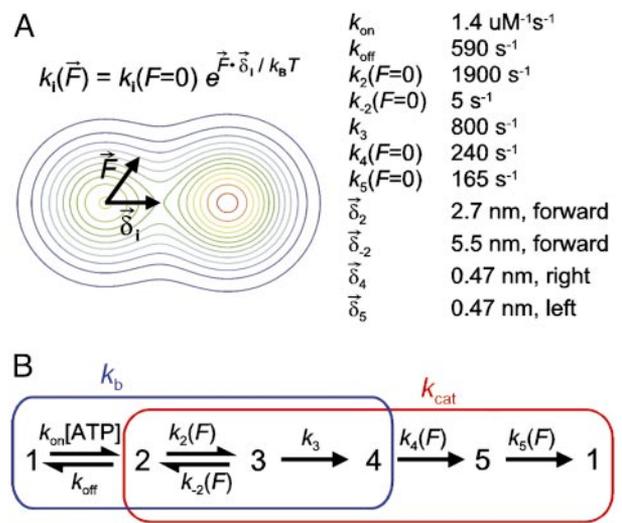
r values. (Histograms were not used in this case, because *r* values are not normally distributed.)

Displacement records obtained for sideways loads included a brief initial relaxation period (roughly exponential, with time constant <30 ms) as the applied force caused the kinesin-bead linkage to move to a new equilibrium orientation perpendicular to the microtubule long axis. To ensure that this relaxation did not influence the velocity determinations for these runs, the *x*- and *y*-displacements vs. time were fit to the sum of an exponential plus a line $\{y(t) = A\exp[-(t - t_0)/\tau] + mt + b\}$, and the slopes, *m*, were used to provide the velocity. We confirmed that this method yielded accurate velocities by performing control experiments in which kinesin-coated beads were tethered to microtubules in the presence of the nonhydrolyzable ATP analog AMP-PNP (2 mM), and moved at 650 nm·s^{-1} with the piezo stage. Force clamping, data collection, and velocity analysis were performed on these tethered beads in exactly the same manner as for kinesin-driven beads. Control determinations of velocity were within 2% of their nominal values for tethered beads clamped under low (1 pN) and high (5 pN) force conditions, for both leftward and rightward forces.

To control for possible artifacts arising from asymmetry in the optical trap itself or in the data collection/analysis, we sampled both sides of the trap at every force condition and ATP concentration, by collecting ≥29 records of motion for each of two opposite microtubule orientations. Records taken in the two orientations were analyzed separately to confirm that any trap asymmetry had a negligible affect on the results (see Fig. 3*C*). For comparison with the force clamp data, kinesin velocities in the absence of external loads were measured by sub-pixel-resolution video tracking of the centroids of beads (13) by using a commercial video tracking software package (ISee Imaging Systems, Raleigh, NC).
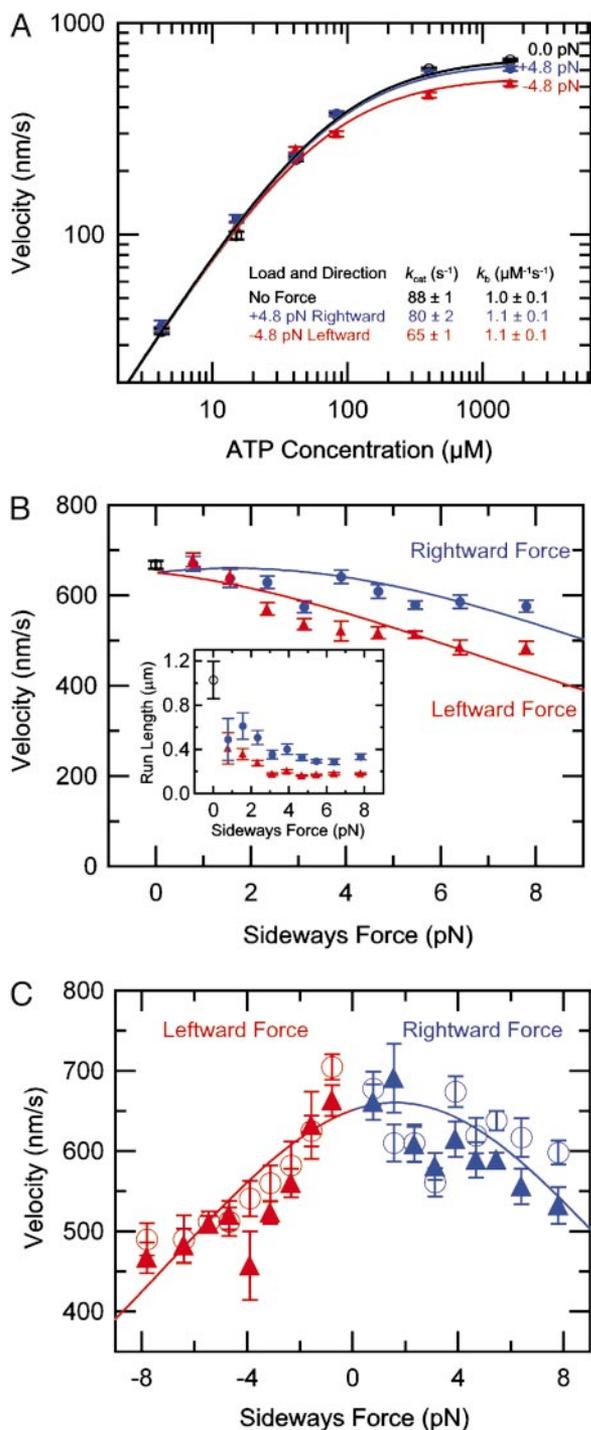
Fig. 3. The effect of sideways load on kinesin velocity. (A) Double-logarithmic plot of average bead velocity (mean ± SEM) vs. ATP concentration for different loading directions (black open circles, no force, $n = 25$–280; blue filled circles, 4.8 ± 0.1 pN rightward force, $n = 29$–99; red triangles, 4.8 ± 0.1 pN leftward force, $n = 33$–113). To derive the rate parameters, data were fit to the MM equation, $V = (8.2 \text{ nm}) \cdot k_{cat}[\text{ATP}]/([\text{ATP}] + k_{cat}/k_b)$. (B) Velocity (mean ± SEM) vs. applied sideways load at 1.6 mM ATP (black open circles, no force, $n = 280$; blue filled circles, rightward force, $n = 87$–142; red triangles, leftward force, $n = 77$–178). (Inset) Run length (mean ± SEM) vs. applied sideways load at 1.6 mM ATP (black open circle, no force, $n = 56$; blue filled circles, rightward force, $n = 87$–142; red triangles, leftward force, $n = 77$–178). (C) Velocity (mean ± SEM) vs. applied sideways load at 1.6 mM ATP for microtubules with their plus-ends pointing up (filled triangles, $n = 29$–105), or down (open circles, $n = 35$–81). Curves in A–C represent the global fit to the five-state model of Fig. 2B (see Discussion).

Mean run lengths (L) were computed as described in ref. 1: L was calculated from $L = \bar{L} + R(1 - f)/f$, where $\bar{L}$ is the average run length, and f is the fraction of runs that terminated inside the limited detector region ($R \approx 300$ nm).

At each load, K_M was calculated from the ratio of the velocity at high ATP to the velocity at low ATP (similar to ref. 14) by using the following formula:

$$K_M = \frac{[\text{ATP}_{high}] \cdot [\text{ATP}_{low}] \cdot (1 - v_{high}/v_{low})}{[\text{ATP}_{low}] \cdot v_{high}/v_{low} - [\text{ATP}_{high}]}. \qquad [\mathbf{1}]$$

Modeling of Data. Our randomness parameter, r, is equivalent to $2D \cdot d^{-1} \langle v \rangle^{-1}$, where D represents the effective diffusion coefficient in a hopping model that corresponds to Markov transitions among enzyme states (15). We therefore used the general expressions for the velocity and diffusion constant in a 1D hopping model to generate predicted force-velocity and force-randomness curves for various N-state, unbranched biochemical cycles. To model the force-dependence of individual transitions within the reaction cycle, exponential Arrhenius–Boltzmann factors with characteristic distances were included in the expressions for the rate constants of selected transitions (Fig. 2; Eq. **1**). Global fits to the data were produced by using the Levenberg–Marquardt algorithm (in IGOR PRO 4.0). Several different models are able to generate satisfactory fits (see Discussion).

Results

Sideways Loads Have an Asymmetric Effect on k_{cat}. We first used the 2D optical force clamp (Fig. 1; see also ref. 7) to study kinesin velocity as a function of ATP concentration under fixed sideways loads. For comparison purposes, unloaded velocities at each ATP concentration were also obtained by subpixel video tracking (see Materials and Methods). Fig. 3A shows that velocities followed MM kinetics under leftward and rightward loads of 4.8 pN, as well as under negligible load. Compared with the unloaded case, sideways loads in either direction lowered k_{cat}, the maximum stepping rate at saturating ATP ([ATP] $\gg K_M = k_{cat}/k_b$), but did not affect k_b, the apparent rate constant for ATP binding (Fig. 3A Inset). This behavior is distinct from what occurs under backward loads, which reduce both k_{cat} and k_b (see ref. 16 and below). The effect of sideways loads on k_{cat} was asymmetric, with leftward loads causing a greater reduction in speed (26%) than rightward loads (9%). Here, "leftward" and "rightward" refer to the direction of loading as seen by an observer facing in the direction of motion along the microtubule (Fig. 1).

The left/right asymmetry was further investigated by measuring velocity at a high ATP level (1.6 mM) as a function of sideways load. Increasing leftward forces from −0.8 to −7.8 pN caused kinesin velocity to decrease by ≈30% relative to its unloaded speed of 668 ± 8.5 nm·s⁻¹ (mean ± SEM; Fig. 3B). Most of this decrease occurred between −0.8 and −3.9 pN, with the velocity nearly leveling off between −3.9 and −7.8 pN. Even the highest leftward loads (−7.8 pN) did not induce stall. Behavior under rightward forces was essentially the same, except that the velocity decreased by only ≈15%. The shape of the sideways force-velocity curve, especially the absence of stall, contrasts sharply with the behavior seen under backward loading (refs. 16–19 and below). Mean run lengths estimated from these data provided further confirmation that the asymmetry was genuine: increasing sideways force in either direction resulted in shorter runs, but leftward loads consistently produced a greater diminution in run length than rightward loads, regardless of microtubule orientation (Fig. 3B Inset).

As a control to ensure that the left/right asymmetry is not an artifact introduced by the apparatus itself or due to an asymmetry in the shape of the optical trap, kinesin motion was recorded for microtubules oriented in diametrically opposing

directions (see *Materials and Methods*). By measuring multiple runs at each orientation, both sides of the optical trap could be sampled for each force condition. Average velocities (Fig. 3*C*) and run lengths for both orientations agreed within experimental uncertainty, and the identical left/right asymmetry was observed in either case.

Forward Loads Do Not Produce a Large Velocity Increase. We next used the force clamp to measure kinesin velocity under constant loads in both forward and backward directions along the microtubule. Kinesin velocity varied sigmoidally with longitudinal load (refs. 1 and 16; Fig. 4*A*). Forward loads between 0.5 and 4.7 pN had no significant effect on velocity at high ATP levels. Similarly, velocity at low ATP levels (4.2 μM) plateaued for forward loads between 2.1 and 7.9 pN. Backward loads at both these ATP concentrations caused the velocity to decrease sharply, dropping to near zero between -4 and -6 pN. Overall, the longitudinal force-velocity curves displayed different shapes at low and high ATP levels. The force required to produce half-maximal velocity, $F_{1/2}$, increased from roughly -2 pN at 4.2 μM ATP to about -4 pN at 1.6 mM ATP. This property directly reflects the different load dependencies of the binding and catalytic rates: k_b decreases more steeply with load than k_{cat} (1, 16). Equivalently, their ratio, K_M, increases with load even as the enzyme slows and k_{cat} drops. The phenomenon is illustrated by comparing the data in Fig. 4 *A* and *B*, which show that K_M increases while the motor speed decreases for saturating ATP under backward load. Apart from a somewhat lower maximal velocity and stall force, the results reported here for backward loads are in close agreement with ref. 16. One recent study (14) found K_M to be independent of load over the range of -1 to -5 pN. The authors suggested that this result may be due to their use of an alternative method to calculate the stepping rate: rather than compute the average velocity for every trace, they measured individual dwell times for the 8-nm steps. However, in our hands, the dwell-time method yields rates that are statistically indistinguishable from the average velocity method, and therefore cannot account for the discrepancy.

We also did not confirm the findings of Coppin *et al.* (17), who reported dramatic increases in kinesin velocity when subjected to time-varying forward loads ($\approx$50% at 1 mM ATP and >300% for 40 μM ATP). There are several sources of concern regarding these data. First, the comparatively lower spatiotemporal resolution of their apparatus may have led the authors inadvertently to process records during which the bead "skipped" forward undetected while subjected to the assisting loads. We often observed such saltatory events, in which the continuous, stepwise motion of the bead was interrupted by a large forward jump ($\gg$8 nm, the unitary step size): sections of records containing jumps were excluded from analysis. These almost certainly represent brief dissociations of the kinesin molecule, leading to trap-driven displacement of the bead, followed by reattachment of the motor to the microtubule. If included in the analysis, jumps raise the apparent motor velocity. Second, because the earlier study was conducted without the benefit of a force clamp, a fairly large compliance correction was applied to the data, which may have introduced further errors: such corrections are unnecessary with a feedback arrangement (20). Finally, we note that the unloaded kinesin velocity reported in ref. 17 was anomalously slow ($\approx$190 nm·s^{-1} at negligible load) compared with native kinesin purified in other labs from the same and other sources [typically 600–800 nm·s^{-1} (16, 18, 19, 21)].

Fluctuation Analysis Indicates Four or More States in Cycle. To determine the apparent number of slow, rate-determining transitions in the kinesin cycle, we performed a statistical fluctuation analysis of records of kinesin motion taken under longitudinal loads. The randomness parameter, r, provides a convenient
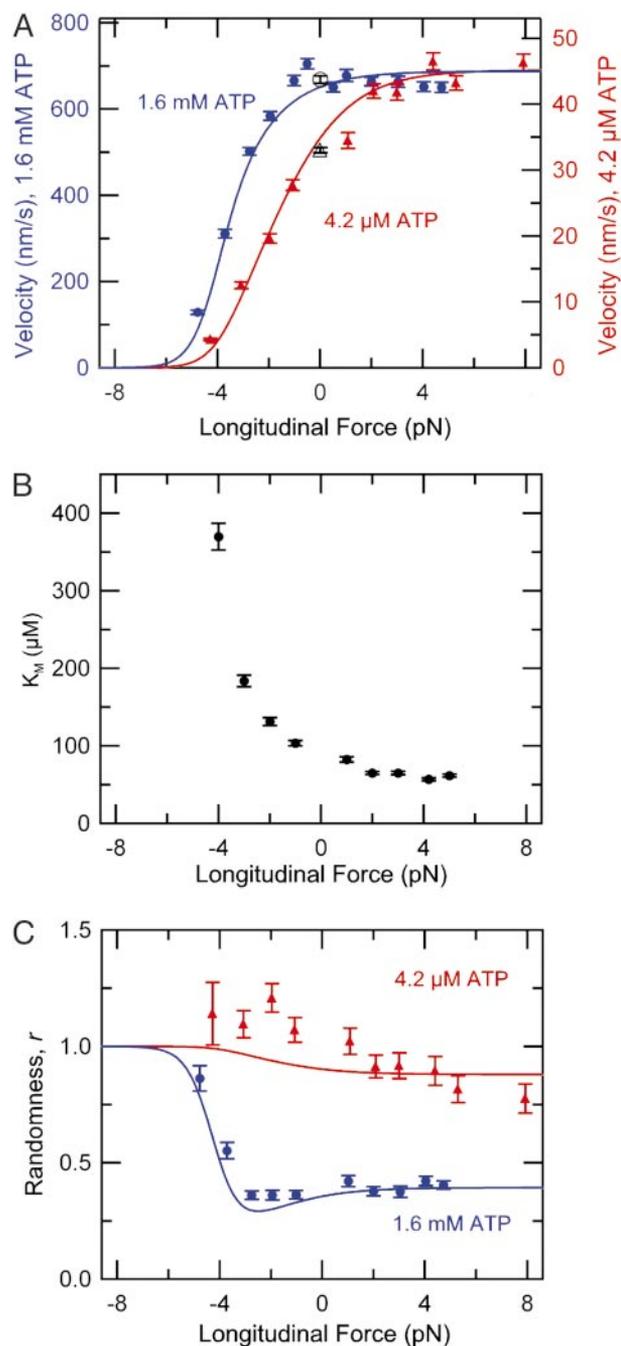

Fig. 4. The effect of longitudinal load on kinesin velocity and randomness. (*A*) Average bead velocity (mean ± SEM) vs. applied longitudinal load for fixed ATP concentrations (red triangles, right axis, 4.2 μM ATP, n = 44–115; blue circles, left axis, 1.6 mM ATP, n = 50–190). Video-tracked data under no external load are also displayed (black open triangles, 4.2 μM ATP, n = 280; open circles, 1.6 mM ATP, n = 58). (*B*) The Michaelis constant, K_M, vs. applied load, calculated from the ratio of velocities shown in *A* (see *Materials and Methods*). (*C*) The randomness parameter, r (mean ± SEM), vs. longitudinal load for fixed ATP concentrations (red triangles, 4.2 μM ATP, n = 44–110; blue circles, 1.6 mM ATP, n = 50–165). Curves in *A* and *C* represent the global fit to the five-state model of Fig. 2*B* (see *Discussion*).

measure of the stochastic variability of the motion (8, 22). We computed this parameter as a function of applied longitudinal force at both low and high ATP concentrations. For processes that consist of a linear sequence of random (Poisson-distributed) events, such as a biochemical cycle, r^{-1} supplies a continuous

measure of the number of slow, rate-determining events. Values of r near unity were obtained at the very lowest concentrations of ATP (4.2 μM), where the binding of an ATP molecule is expected to be the single rate-determining event in the cycle (ref. 8; Fig. 4C, red triangles). Values of r slightly above unity obtained for backward loads are consistent with the small fraction of backsteps found to occur under these conditions: roughly 2–5% of all steps taken under backward loading at limiting ATP concentrations were rearward. No such backward steps were seen for forward loading.

At 1.6 mM ATP, nucleotide binding is greatly accelerated, and other events in the cycle become rate-determining. The presence of more than one rate-determining event results in more statistically regular motion and lowered r values (Fig. 4C, blue circles). Over the force range from −3 pN to +5 pN, r values were nearly constant, close to 0.38 ± 0.01 (mean ± SEM). These numbers are in excellent agreement with those published previously for backward loads alone (16). The value of $r \approx 1/3$ implies that the kinesin cycle contains at least three more transitions, in addition to the ATP binding step that is rate-determining at limiting ATP levels. Furthermore, the invariance of r with load indicates that the coupling of ATP hydrolysis to stepping remains tight over the entire range of loads (16).

Discussion

Kinesin motor behavior depends strongly on the direction of loading. Sideways loads slowed the motor asymmetrically, causing a greater decrease in velocity when applied to the left (26%) than to the right (9%), but only when ATP levels were not limiting ([ATP] > 80 μM). However, sideways forces even as large as ±8 pN failed to induce stall. Single kinesin motors did not exhibit large changes in speed when subjected to forward (assisting) loads, showing at most a 40% increase relative to the unloaded speed at 4.6 μM ATP, and no significant increase at 1.6 mM ATP, contrary to one earlier report (17). The longitudinal force-velocity relationship was sigmoidal, with the velocity reaching a plateau under forward loads. In contrast, increasing the backwards load produced a sharp drop in kinesin speed and led to stall between −4 and −6 pN. These findings impose constraints on the kinesin biochemical reaction cycle, and specifically on the transitions in the cycle whose rates are load-dependent.

Kinesin motors do not advance with clock-like regularity. Analysis of deviations from regularity reveals that at least four transitions in the underlying mechanochemical cycle can become rate-determining. We quantified the irregularity of kinesin motion using the randomness parameter, r, a dimensionless parameter related to the relative variance about the average trajectory (8, 22, 23). Kinesin stepping rates at limiting ATP concentrations ([ATP] $\ll K_M$) are governed by the arrival and productive binding of single nucleotides. Consequently, the motor behaves in this regime as a Poisson stepper, with exponentially distributed step intervals and a large variance, leading to randomness values near unity (Fig. 4C, red triangles; see also refs. 8 and 16). At high ATP levels, the stepping process becomes more regular, and randomness is reduced to $r = 0.38 \pm 0.01$ (average ± SEM.) over a very wide range of longitudinal loads (from −3 pN to +5 pN; Fig. 4C, blue circles). The experimental value for r^{-1} (2.6 $\approx$ 3) implies that there are at least three slow events limiting the overall cycle time. These three events, taken together with the reaction step that corresponds to the binding of ATP (which is too fast in this particular regime to affect kinetics), comprise a total of four potentially rate-determining transitions. This number represents a lower bound: a minimal model for kinesin kinetics must therefore include at least four transitions. This limit seems reasonable, because more than four biochemical events are known to occur for each 8-nm step that kinesin takes, for example, microtubule attachment, ATP binding, ATP hy-

drolysis, release of ADP and phosphate, microtubule detachment, etc.

The effect of load on the MM parameters k_{cat} and k_b indicates that the kinesin reaction cycle contains more than one load-dependent transition, and it places constraints on reaction schemes that may be considered. Experimentally, velocities measured for kinesin exhibit MM dependence on the ATP concentration, even under longitudinal (16) and sideways loads (Fig. 3A). Sideways loads were found to affect only the turnover parameter, k_{cat}. Not all reaction schemes contain rates affecting only k_{cat}, but in pathways with two irreversible transitions, for example, the second such transition satisfies the requirement. Both k_4 and k_5 in Fig. 2 have this property. Longitudinal loads reduce both k_{cat} and k_b (ref. 16 and this work). The two effects of longitudinal load may be explained by a single load-dependent rate, because at least one of the microscopic rates of any multistep reaction cycle obeying MM kinetics affects both k_{cat} and k_b (i.e., the overlap rates). However, if one assumes that a single load-dependent transition is responsible for all of the effects of longitudinal load, that same transition cannot also account for sideways loads, where only k_{cat} is lowered. Therefore, at least two load-dependent transitions are required in a minimal scheme, regardless of the exact details of the biochemical reaction.

Could either of the two putative load-dependent transitions constitute a "working stroke," and if so, what is the nature of the transition? Based on numerical comparisons with a number of candidate reaction schemes (below), our data are consistent with the existence of a working stroke that occurs early in the cycle, directed (productively) along the microtubule, in addition to smaller motions later in the cycle. For simplicity, we considered only 4- and 5-state, unbranched pathways, beginning with a reversible ATP-binding step. Incorporating at least two irreversible transitions elsewhere in the pathway guaranteed that all schemes contained at least one rate affecting only k_{cat} (necessary to accommodate the effect of sideways load), and also ensured MM dependence on ATP concentration. Rather than allowing all transitions to carry force dependence (24), we sought a model with a minimal number of such transitions. Force dependence in one or more rates was assumed to result from changes in the height of an energy barrier as the energy landscape is tilted by the application of load. Thus, the force-dependent rates incorporate an Arrhenius–Boltzmann factor, $\exp(\vec{F} \cdot \vec{\delta}_i/k_BT)$, where $\vec{\delta}_i$ is the vector from the ith starting state to its transition state along the reaction coordinate, and $\vec{F}$ is the corresponding vector of applied force (see Fig. 2). Given a reaction pathway and its rates, general expressions have been derived for computing the mean velocity and also the randomness (15). Fits to our data were obtained by adjusting all unloaded rates and δ_is to minimize the global χ^2 sum for velocity and randomness as functions of ATP concentration and force. Generally, the best fits were produced by models in which one overlap rate had a strong longitudinal force dependence (so that both k_{cat} and k_b were affected by longitudinal load) plus additional rates later in the cycle that incorporated weak sideways force-dependencies, so that k_{cat} could be affected by sideways load.

One model that fits the data well is displayed in Fig. 2 (curve fits are shown as solid lines in Figs. 3 and 4). The shapes of the longitudinal force-velocity and force-randomness curves are dominated by $k_2(F)$, the forward rate for the 2→3 transition, which supplies a 2.7-nm motion (δ_2) directed toward the plus-end of the microtubule, from state 2 to its transition state. Backward loads decrease $k_2(F)$, which can become rate-determining and thereby slow the stepping rate. Forward loads accelerate $k_2(F)$, but these cannot increase the overall motor speed significantly, because other, force-independent transitions in the cycle limit the overall stepping rate. The remaining 5.5 nm of the 8.2-nm step along the microtubule occur between the transition state

and state 3, and supply force-dependence to the backwards rate, $k_{-2}(F)$. This force-dependence has little effect on the overall stepping rate, because $k_{-2}(F)$ remains small compared with $k_3(F)$ for most loading conditions, except near stall ($F > 3$ pN). The relatively weak effect of sideways load on motor velocity is developed through the last two transitions, $k_4(F)$ and $k_5(F)$, which include small (0.47 nm) lateral motions that are equal in magnitude and opposite in direction. Leftward loads decrease $k_4(F)$ but increase $k_5(F)$, whereas rightward loads have the reciprocal effect, the net effect being a slight decrease in velocity under either leftward or rightward force.

Certain features of this reaction scheme are similar to those of a model presented previously (1). Both pathways include a critical load-dependent transition in the overlap region, where k_{cat} and k_b are both affected, with longitudinal force-dependence described by an energy-landscape formalism, acting over a 3- to 4-nm characteristic distance. The current model does not postulate a composite state (1), however, although it generates force-velocity and ATP-velocity curves with rather similar shapes. The present model also accounts fully for the force-randomness data (Fig. 4C). In contrast, this particular model predicts no detectable substeps, because the full 8.2-nm step occurs during a single mechanical transition. However, our data can also be satisfactorily fit by a reaction pathway in which the 5.5-nm motion occurs later in the cycle, for example, on any reverse rate constant that is slow enough not to affect the kinetics. Therefore, conclusions should not be drawn from these data about the possible existence of substeps.

What do the current measurements say about the conformational changes that drive motility? Despite the requirement for multiple, force-dependent transitions to explain the effects of all azimuthal loads, we believe that an (essentially) one-stroke mechanism remains the best explanation for the available data. The effect of sideways loads is comparatively weak, and can be accommodated by minor transverse load-dependencies later in the cycle, perhaps occurring concomitant with ADP and/or P_i release. In contrast, the sharp stalling behavior under backward load requires a strong load dependence that acts early in the cycle, and is most easily modeled by a large conformational change occurring at a transition affecting both k_{cat} and k_b. To be consistent with the negligible effect of sideways load on k_b, this hypothetical power stroke must be well-aligned with the microtubule long axis. Further experiments in which the effects of P_i and ADP concentrations are explored, or in which the binding/release of fluorescent nucleotide analogues is observed, may identify the specific chemical reactions that correspond to the load-dependent and load-independent transitions within the cycle.

1. Schnitzer, M. J., Visscher, K. & Block, S. M. (2000) *Nat. Cell Biol.* **2,** 718–723.
2. deCastro, M. J., Fondecave, R. M., Clarke, L. A., Schmidt, C. F. & Stewart, R. J. (2000) *Nat. Cell Biol.* **2,** 724–729.
3. Rice, S., Lin, A. W., Safer, D., Hart, C. L., Naber, N., Carragher, B. O., Cain, S. M., Pechatnikova, E., Wilson-Kubalek, E. M., Whittaker, M., *et al.* (1999) *Nature* **402,** 778–784.
4. Svoboda, K., Schmidt, C. F., Schnapp, B. J. & Block, S. M. (1993) *Nature* **365,** 721–727.
5. Sindelar, C. V., Budny, M. J., Rice, S., Naber, N., Fletterick, R. & Cooke, R. (2002) *Nat. Struct. Biol.* **9,** 844–848.
6. Block, S. M. (1995) *Trends Cell Biol.* **5,** 169–175.
7. Lang, M. J., Asbury, C. L., Shaevitz, J. W. & Block, S. M. (2002) *Biophys. J.* **83,** 491–501.
8. Schnitzer, M. J. & Block, S. M. (1997) *Nature* **388,** 386–390.
9. Hackney, D. D. (1994) *J. Biol. Chem.* **269,** 16508–16511.
10. Gilbert, S. P., Webb, M. R., Brune, M. & Johnson, K. A. (1995) *Nature* **373,** 671–676.
11. Ma, Y. Z. & Taylor, E. W. (1995) *Biochemistry* **34,** 13233–13241.
12. Vale, R. D., Reese, T. S. & Sheetz, M. P. (1985) *Cell* **42,** 39–50.
13. Gelles, J., Schnapp, B. J. & Sheetz, M. P. (1988) *Nature* **331,** 450–453.
14. Nishiyama, M., Higuchi, H. & Yanagida, T. (2002) *Nat. Cell Biol.* **4,** 790–797.
15. Derrida, B. (1983) *J. Stat. Phys.* **31,** 433–450.
16. Visscher, K., Schnitzer, M. J. & Block, S. M. (1999) *Nature* **400,** 184–189.
17. Coppin, C. M., Pierce, D. W., Hsu, L. & Vale, R. D. (1997) *Proc. Natl. Acad. Sci. USA* **94,** 8539–8544.
18. Kojima, H., Muto, E., Higuchi, H. & Yanagida, T. (1997) *Biophys. J.* **73,** 2012–2022.
19. Meyhofer, E. & Howard, J. (1995) *Proc. Natl. Acad. Sci. USA* **92,** 574–578.
20. Visscher, K. & Block, S. M. (1998) *Methods Enzymol.* **298,** 460–489.
21. Hua, W., Young, E. C., Fleming, M. L. & Gelles, J. (1997) *Nature* **388,** 390–393.
22. Schnitzer, M. J. & Block, S. M. (1995) *Cold Spring Harbor Symp. Quant. Biol.* **60,** 793–802.
23. Svoboda, K., Mitra, P. P. & Block, S. M. (1994) *Proc. Natl. Acad. Sci. U.S.A.* **91,** 11782–11786.
24. Fisher, M. E. & Kolomeisky, A. B. (2001) *Proc. Natl. Acad. Sci. USA* **98,** 7748–7753.